Journal of Heat Transfer Published by ASME

Dear Author,

Congratulations on having your paper accepted for publication in the ASME Journal Program.

Your page proof is available in PDF format from the ASME Proof Download & Corrections site here:

http://115.111.50.156/jw/AuthorProofLogin.aspx?pwd=a0ab25993059&CA=AS

Login: your e-mail address

Password: a0ab25993059

Please keep this email in case you need to refer back to it in the future.

You will need Adobe Acrobat Reader software to view the file. This is free software and a download link is provided when you log in to view your proofs.

Responsibility of detecting errors rests with the author. Please review the page proofs carefully and:

1. Answer any queries on the first page "Author Query Form"
2. Proofread any tables and equations carefully
3. Check to see that any special characters have translated correctly
4. Publication will not proceed until a response is received. If there are no corrections, a response is still required.

RETURNING CORRECTIONS:

Corrections must be returned using the ASME Proof Download & Corrections Submission Site (link above). You will be able to upload:

1. Annotated PDF
2. Text entry of corrections, with line numbers, in the text box provided
3. Additional files, if necessary.

SPECIAL NOTES:

Your Login and Password are valid for a limited time. Please reply within 48 hours.

Corrections not returned through the above website will be subject to publication delays. This e-proof is to be used only for the purpose of returning corrections to the publisher. If you have any questions, please contact: asme.cenveo@cenveo.com, and include your article no. (HT-16-1093) in the subject line. This email should not be used to return corrections.

Approval of these proofs re-confirms the copyright agreement provision that all necessary rights from third parties for any copyrighted material (including without limitation any diagrams, photographs, figures or text) contained in the paper has been obtained in writing and that appropriate credit has been included.

Sincerely,

Kim Ross, Journal Production Manager

STATEMENT OF EDITORIAL POLICY AND PRACTICE

The Technical Committee on Publications and Communications (TCPC) of ASME aims to maintain a high degree of technical, literary, and typographical excellence in its publications. Primary consideration in conducting the publications is therefore given to the interests of the reader and to safeguarding the prestige of the Society.

To this end the TCPC confidently expects that sponsor groups will subject every paper recommended by them for publication to careful and critical review for the purpose of eliminating and correcting errors and suggesting ways in which the paper may be improved as to clarity and conciseness of expression, accuracy of statement, and omission of unnecessary and irrelevant material. The primary responsibility for the technical quality of the papers rests with the sponsor groups.

In approving a paper for publication, however, the TCPC reserves the right to submit it for further review to competent critics of its own choosing if it feels that this additional precaution is desirable. The TCPC also reserves the right to request revision or condensation of a paper by the author or by the staff for approval by the author. It reserves the right, and charges the editorial staff, to eliminate or modify statements in the paper that appear to be not in good taste and hence likely to offend readers (such as obvious advertising of commercial ventures and products, comments on the intentions, character, or acts of persons and organizations that may be construed as offensive or libelous), and to suggest to authors rephrasing of sentences where this will be in the interest of clarity. Such rephrasing is kept to a minimum.

Inasmuch as specific criteria for the judging of individual cases cannot, in the opinion of the TCPC, be set up in any but the most general rules, the TCPC relies upon the editorial staff to exercise its judgment in making changes in manuscripts, in rearranging and condensing papers, and in making suggestions to authors. The TCPC realizes that the opinions of author and editor may sometimes differ, and hence it is an invariable practice that no paper is published until it has been passed on by the author. For this purpose page proofs of the edited paper are sent to the author prior to publication in a journal. Changes in content and form made in the proofs by authors are followed by the editor except in cases in which the Society's standard spelling and abbreviation forms are affected.

If important differences of opinion arise between author and editor, the points at issue are discussed in correspondence or interview, and if a solution satisfactory to both author and editor is not reached, the matter is laid before the TCPC for adjustment.

Technical Committee on Publications and Communications (TCPC)
Reviewed: 05/2012

AUTHOR QUERY FORM

ASME SETTING THE STANDARD	Journal: J. Heat Transfer Article Number: HT-16-1093	Please provide your responses and any corrections by annotating this PDF and uploading it to ASME's eProof website as detailed in the Welcome email.

Dear Author,

Below are the queries associated with your article; please answer all of these queries before sending the proof back to Cenveo. Production and publication of your paper will continue after you return corrections or respond that there are no additional corrections.

Location in article	Query / Remark: click on the Q link to navigate to the appropriate spot in the proof. There, insert your comments as a PDF annotation.
AQ1	Reminder – the ASME Copyright Agreement that was signed by all authors includes the following: "You have the right to enter into this Copyright Form and to make the assignment of rights to ASME. If the Paper contains excerpts from other copyrighted material (including without limitation any diagrams, photographs, figures or text), you have acquired in writing all necessary rights from third parties to include those materials in the Paper, and have provided appropriate credit for that third-party material in footnotes or in a bibliography." As required, ASME may contact the authors to obtain a copy of the written permission.
AQ2	Any content obtained from the web and included in the paper may require written permission and appropriate credit if it is copyrighted content. If copyright status cannot be determined, this content should not be included in the paper.
AQ3	Please check the presentation of all affiliations.
AQ4	Please reword the sentence beginning with "In special, near-infrared" so that your meaning will be clear to the reader.
AQ5	References must be cited in numerical order. Please check renumbering of Refs. 67–70.
AQ6	Please provide publisher location for Refs. 6, 12, 49, and 61.
AQ7	Please provide paper no. or page number in range for Ref. 7.
AQ8	Please provide publisher name and location for Refs. 9 and 67.
AQ9	Please provide year for Ref. 16.
AQ10	Please check edits made in Refs. 9, 26, 49, 60, and 67.
AQ11	Please provide volume number and page number in range for Ref. 27.
AQ12	Please update Refs. 28 and 29 with volume number, issue number, page number, and year if published.
AQ13	"et al." is not permitted in the reference list. Please provide the full list of authors for Refs. 44 and 54.
AQ14	Please provide location for Refs. 16 and 70.
AQ15	Please provide DOI for Refs. 24, 56, 60 and 63.

Thank you for your assistance.

AQ1
AQ2
AQ3

Bernard Lamien
Department of Mechanical Engineering,
DEM/PEM—Politecnica/COPPE,
Federal University of Rio de Janeiro—UFRJ,
Cidade Universitária,
Caixa Postal: 68503,
Rio de Janeiro, RJ 21941-972, Brazil
e-mail: lamienbernard@hotmail.com

Helcio Rangel Barreto Orlande[1]
Department of Mechanical Engineering,
DEM/PEM—Politecnica/COPPE,
Federal University of Rio de Janeiro—UFRJ,
Cidade Universitária,
Caixa Postal: 68503,
Rio de Janeiro, RJ 21941-972, Brazil
e-mail: helcio@mecanica.coppe.ufrj.br

Guillermo Enrique Eliçabe
Institute of Materials Science and Technology
(INTEMA),
University of Mar del Plata and National
Research Council (CONICET),
J. B. Justo 4302,
Mar del Plata 7600, Argentina
e-mail: elicabe@fi.mdp.edu.ar

Particle Filter and Approximation Error Model for State Estimation in Hyperthermia

This work deals with numerical simulation of a hyperthermia treatment of skin cancer as a state estimation problem, where uncertainties in the evolution and measurement models, as well as in the measured data, are accounted for. A reduced model is adopted, based on a coarse mesh for the solution of the partial differential equations that describe the physical problem, in order to expedite the solution of the state estimation problem with a Particle Filter algorithm within the Bayesian framework of statistics. The so-called approximation error model (AEM) is used in order to statistically compensate for model reduction effects. The Liu and West algorithm of the Particle Filter, together with the AEM, is shown to provide accurate estimates for the temperature and model parameters in a multilayered region containing a tumor loaded with nanoparticles. Simulated transient temperature measurements from one sensor are used in the analysis.
[DOI: 10.1115/1.4034064]

Introduction

State estimation problems have a broad range of applications, including telecommunications, navigation, and biology, to name a few. In state estimation problems, the available measured data are used together with mathematical models for the physical phenomena and the measuring devices, in order to sequentially produce estimates of the desired dynamic variables. This is generally accomplished within a probabilistic framework, where the solution of the state estimation problem consists of sequential estimations of posterior probability densities of the state variables, through the use of Bayesian filters [1–3]. As new data become available, the posterior probability distribution is updated so that it reflects the current state of the system. Unlike the Kalman filter or its extensions, Particle Filters do not rely on any local linearization or any prior assumption about the posterior probability density [1–3].

Particle Filters make use of the importance sampling technique, which is a generalization of the Monte Carlo method for nonexplicit probability density functions. The posterior probability density, which is the target of the solution of the state estimation problem, is then represented by a set of samples, referred to as particles, with associated weights [1–3]. Different Particle Filter algorithms can be encountered in the literature, including the sampling importance resampling and the auxiliary sampling resampling filters. These Particle Filter algorithms may fail in providing simultaneous estimates of the state variables and of the nondynamic model parameters [4]. Thus, they are mainly used by assuming that the nondynamic parameters are deterministically known. However, in most practical applications, the parameters appearing in the mathematical formulation might be unknown, or at most known with some degree of uncertainty. The problem of simultaneous estimation of state variables and of nondynamic model parameters can be handled with the algorithm developed by Liu and West [4], also known as Kernel density particle filter [5]. In addition to the Liu and West algorithm of the Particle Filter, other algorithms were proposed to address such kind of problem [6]. However, the Liu and West algorithm is more general and can be considered as a benchmark in the current literature [6].

Though very robust, the computational cost related to the use of Particle Filter methods is generally high due to their Monte Carlo nature. Indeed, their use for state estimation involving complex physical simulations can be prohibitive, especially for applications where there is a time constraint for control or decision making. Attempts to reduce the computational cost of Particle Filter methods include parallelization [7–10] and model reduction [11]. In fact, the proposed statistical model reduction technique referred to as AEM [12–25] has been recently coupled with the Liu and West filter in order to accelerate the solution of a state estimation problem applied to a one-dimensional hyperthermia problem [11].

Planning and/or predictive control of the hyperthermia treatment of cancer can greatly benefit from the Bayesian state estimation formalism in order to provide more reliable and individualized protocols. Indeed, tissues' physical properties and geometries present a large variability from an individual to another, or even for the same individual under different physiological conditions. Hence, the input data needed for numerical simulations involving biological tissues are highly uncertain [11,26–34].

Hyperthermia is a current research topic, highly influenced by recent progresses in nanotechnology. Minimally invasive therapies for cancer constitute a great motivation for the use of nanoparticles in combination with traditional therapies. In fact, the subcellular size and the physical properties of nanoparticles make them good candidates for novel therapies. Particularly in the near-infrared photo-thermal therapy of cancer, nanoparticles with strong absorption properties are used to enhance local heat deposition in cancerous regions [35–42]. This treatment modality is often used as adjuvant to radiotherapy or chemotherapy, in order to improve their efficiencies [42,43]. In special, near-infrared photo-thermal therapy of cancer was suggested for superficial tumors,

[1]Corresponding author.

Contributed by the Heat Transfer Division of ASME for publication in the Journal of Heat Transfer. Manuscript received February 18, 2016; final manuscript received June 25, 2016; published online xx xx, xxxx. Assoc. Editor: Dr. Portonovo S. Ayyaswamy.

AQ4

like skin cancer, due to the limited penetration depth of laser light in tissues [39]. Other topics of current research related to the photo-thermal hyperthermia treatment of cancer include the excretion and toxicology of nanoparticles (see, for example, Refs. [44–46] for the development of biodegradable nanoparticles), as well as the quantification of the thermal damage imposed on different types of cells (see Refs. [47] and [48] for discussions and comparative mathematical models of cell thermal damage). Anyhow, reported experimental results and clinical trials have demonstrated the selectivity and the minimally invasive feature of nanoparticles for hyperthermia applications [35–42,44–46,49]. On the other hand, numerical simulations are of major importance in hyperthermia treatment planning and control, in order to minimize damage to normal cells.

This work aims at the application of the Liu and West algorithm of the Particle Filter [4] together with the AEM [12–25] for the solution of an inverse bioheat transfer state estimation problem. The problem aims at the estimation of the temperature in the hyperthermia treatment of a subcutaneous tumor loaded with nanoparticles, by assuming available local temperature measurements from one sensor. Thermophysical and optical properties appearing in the mathematical formulation of the physical problem, which are modeled in terms of a mixture of Gaussian kernels, are also simultaneously estimated together with the temperature field.

Physical Problem and Mathematical Formulation

The physical problem under consideration in this paper involves the hyperthermia treatment of a subcutaneous tumor, induced by an external collimated laser beam under constant illumination (CW) [50,51]. The skin is represented as an inhomogeneous cylindrical medium with five layers, where each layer corresponds to a specific tissue, namely: epidermis, dermis, fat, muscle, and a tumor buried in the dermis (see Fig. 1 for geometry and dimensions). The tumor is assumed to be loaded with gold nanorods in order to enhance the hyperthermia effects and to limit such effects to the tumor region.

The laser radiation propagation in the skin is modeled in this work with the δ-P1 approximation [52,53], even though other more simplified diffusion formulations have been used in the literature for similar cases [54,55]. The laser beam is assumed to be co-axial with the cylindrical skin model so that the problem can be formulated as two-dimensional with axial symmetry. At the external surface of the skin, the incident laser radiation is assumed to be partially reflected (specular reflection), with reflection coefficient R_{sc}. The internal surface of the irradiated boundary is assumed to partially and diffusively reflect the incident radiation, with reflectivity characterized by Fresnel's coefficient A_1, while opacity is assumed for the remaining boundaries. The refractive indexes of the different tissues are assumed constant and homogeneous.

The diffuse component of the fluence rate is given by the following boundary value problem [52]:

$$\nabla\cdot\left[-D(r,z)\nabla\Phi_s(r,z)+\frac{\sigma_s'(r,z)g'(r,z)}{\beta_{tr}(r,z)}\Phi_p(r,z)\hat{\mathbf{s}}_c\right]+\kappa(r,z)\Phi_s(r,z)=\sigma_s'(r,z)\Phi_p(r,z)\quad \text{in } 0<r<L_r \text{ and } 0<z<L_z \tag{1a}$$

$$-D(r,z)\nabla\Phi_s(r,z)\cdot\mathbf{n}+\frac{1}{2A_1}\Phi_s(r,z)=-\frac{\sigma_S'(r,z)g'(r,z)}{\beta_{tr}(r,z)}\Phi_p(r,z)\quad \text{at } z=0,\ 0<r<L_r \tag{1b}$$

$$\Phi_S(r,z)=0\qquad \text{at } z=L_z, 0<r<L_r \tag{1c}$$

$$\nabla\Phi_s(r,z)\cdot\mathbf{n}=0\qquad \text{at } r=0,\ 0<z<L_z \tag{1d}$$

$$\Phi_S(r,z)=0\qquad \text{at } r=L_r,\ 0<z<L_z \tag{1e}$$

where

$$D=\frac{1}{3\beta_{tr}} \tag{2a}$$

$$\sigma_s'=(1-g^2)\sigma_s \tag{2b}$$

$$g'=\frac{g}{1+g} \tag{2c}$$

$$A_1=(1+R_2)/(1-R_1) \tag{2d}$$

$$\beta_{tr}=\kappa+\sigma_s(1-g) \tag{2e}$$

with g being the anisotropic scattering factor, σ_s the scattering coefficient, while R_1 and R_2 are the first and second moments of Fresnel's reflection coefficient, respectively.

The collimated component of the fluence rate follows the generalized Beer–Lambert's law and is given by [52]:

$$\Phi_p(r,z)=\Phi_{0,i}(r,z)=\Phi_{0,i-1}(r,d_{i-1}(r))\exp\left[-\beta_i'(z-z_i)\right] \tag{3a}$$

with

$$\beta'=\kappa+\sigma_s' \tag{3b}$$

where the subscript i refers to the layer i, d_i is the thickness of each layer, while z_i and $\Phi_{0,i-1}$ are the axial position at which the collimated light enters layer i and the collimated fluence rate at this position, respectively. For $i=1$, we have

$$\Phi_{0,1}(r,z)=(1-R_{sc})E(r)\exp(\beta_1'z) \tag{3c}$$

with

$$E(r)=\begin{cases}E_0, & r\le L_{tumor}\\ 0\ , & r>L_{tumor}\end{cases} \tag{3d}$$

The total fluence rate is obtained by adding both diffuse and collimated components, that is,

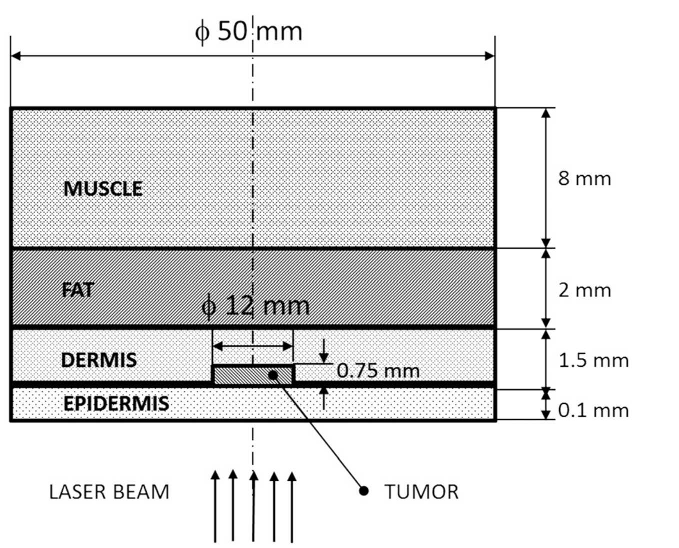

Fig. 1 Sketch of the skin model

$$\Phi(r,z) = \Phi_p(r,z) + \Phi_s(r,z) \tag{4}$$

The heat transfer problem resulting from the laser irradiation of the medium is modeled in terms of the two-dimensional Pennes' equation [56] in cylindrical coordinates with axial symmetry. The internal surface (at $z = L_z$) is assumed to exchange heat with the deeper tissues beyond the computational domain, at a core body temperature T_{int}, with a heat transfer coefficient h_{int}, while the irradiated surface (at $z = 0$) is assumed to be cooled by air in order to avoid overheating of the skin [40,41,57]. The heat transfer coefficient and the temperature of the surrounding medium at $z = 0$ are assumed to vary in the radial direction. Heat transfer is neglected through the lateral surfaces of the medium. The heat transfer problem is then formulated by using position-dependent properties as

$$\rho(r,z)c_p(r,z)\frac{\partial T(r,z,t)}{\partial t} = \nabla \cdot \left[k(r,z)\nabla T(r,z,t)\right] + Q(r,z,t) \qquad 0 < z < L_z,\ 0 < r < L_r\ \ t > 0 \tag{5a}$$

$$k(r,z)\nabla T(r,z,t)\cdot \mathbf{n} + h_c(r)T(r,z,t) = h_c(r)T_c(r), \qquad z = 0\,,\ 0 < r < L_r\ t > 0 \tag{5b}$$

$$k(r,z)\nabla T(r,z,t)\cdot \mathbf{n} + h_{\text{int}}T(r,z,t) = h_{\text{int}}T_{\text{int}}, \qquad z = L_z\,,\ 0 < r < L_r,\ t > 0 \tag{5c}$$

$$\nabla T(r,z,t)\cdot \mathbf{n} = 0,\ r = 0,\ \ 0 < z < L_z\, t > 0 \tag{5d}$$

$$\nabla T(r,z,t)\cdot \mathbf{n} = 0,\ r = L_r,\ 0 < z < L_z\ \ t > 0 \tag{5e}$$

$$T(r,z,t) = T_s(r,z)\ \ 0 < z < L_z,\ \ 0 < r < L_r,\ \ t = 0 \tag{5f}$$

where

$$Q(r,z,t) = \rho_b c_{p,b}\omega_b(r,z)[T_b - T(r,z,t)] + Q_{\text{met}}(r,z) + Q_{\text{laser}}(r,z) \tag{5g}$$

that includes the heat source due to laser absorption

$$Q_{\text{laser}}(r,z) = \kappa(r,z)\Phi(r,z) \tag{5h}$$

as well as the heat source due to metabolism and the effect of blood perfusion. The heat source term Q_{laser} induced by the laser radiation is computed from the fluence rate and the absorption coefficient.

State Estimation

Inverse problems in which the unknowns are time-dependent are referred to as state estimation or nonstationary inverse problems [1–3,6,12,58–62]. This kind of problem can be encountered in several science and engineering applications. In most of these applications, prior knowledge about the physical phenomena being modeled is available [3]. This knowledge allows for the formulation of Bayesian models that involve the prior distributions for the unknown quantities and the likelihood functions relating these quantities to the observations [3]. Within the Bayesian framework, inference on the unknown quantities is based on the posterior probability distribution obtained from Bayes' theorem [3]. Very often, observations are obtained at some discrete time instants and one is interested in obtaining estimates of the unknown quantities as new observations become available. For such cases, nonstationary inverse problems may be written in the form of evolution and observation models given as stochastic processes [1–3,12]. Evolution and observation models inherently incorporate nondynamic parameters, which might be unknown or known with some degree of uncertainty. Thus, these parameters may need to be estimated simultaneously with the state variables.

Let us consider a vector $\mathbf{x}_k$ that contains all the state variables that describe the system at a given time instant t_k. We further assume the state evolution model and the observation model, which are defined by the functions $\mathbf{f}_k$ and $\mathbf{g}_k$, respectively. Thus, we can write the evolution model and the observation model, respectively, as [1–3]

$$\mathbf{x}_k = \mathbf{f}_k(\mathbf{x}_{k-1}, \boldsymbol{\theta}, \mathbf{w}_k), \quad k = 1, \ldots, M \tag{6a}$$

$$\mathbf{z}_k = \mathbf{g}_k(\mathbf{x}_k, \boldsymbol{\theta}, \mathbf{v}_k), \quad k = 1, \ldots, M \tag{6b}$$

where $\boldsymbol{\theta}$ is a vector containing all the nondynamic parameters of the model, while $\mathbf{w}_k$ and $\mathbf{v}_k$ represent the noises in the state evolution model and in the observation model, respectively.

For the state estimation problem under consideration in this work, the state variables in the vector $\mathbf{x}_k = [\boldsymbol{\Phi}_k, \mathbf{T}_k]$ are the fluence rates and temperatures at the centers of the finite volumes used in the discretization of the forward problem, at time t_k, represented by the vectors $\boldsymbol{\Phi}_k$ and $\mathbf{T}_k$, respectively. The vector of nondynamic parameters, $\boldsymbol{\theta}$, contains all the optical and thermophysical parameters appearing in the mathematical formulation of the forward problem given by Eqs. (1)–(5).

Given the state-space models of Eqs. (6a) and (6b), the objective of the state estimation problem is to obtain information about the state vector $\mathbf{x}_k$ by sequentially estimating in time the posterior probability density $\pi(\mathbf{x}_k, \boldsymbol{\theta}|\mathbf{z}_{1:k})$, where $\mathbf{z}_{1:k}$ is the set of all measurements up to time t_k, that is, $\{\mathbf{z}_1, \mathbf{z}_2, \ldots, \mathbf{z}_k\}$. By assuming that the probability density $\pi(\mathbf{x}_0, \boldsymbol{\theta}|\mathbf{z}_0) = \pi(\mathbf{x}_0, \boldsymbol{\theta})$ at the initial time $t = t_0$ is available, the solution of the state estimation problem is obtained with Bayesian filters in two steps: prediction and update [1–3,12,58–61]. The prediction step involves the evolution of the state variables from time instant t_{k-1} to t_k, by using Eq. (6a), while in the update step, the likelihood function, relating the predicted observations and the available observations at t_k, is taken into account. Kalman-like filters approximate the posterior probability density as Gaussian. Though such an approach has proved to be efficient in different applications, it can have severe limitations for highly nonlinear problems. Unlike Kalman filters, sequential Monte Carlo Methods, also referred to as Particle Filters, are more general and do not rely on any local linearization or any prior assumption about the posterior probability density [1–3].

The Particle Filter method is a Monte Carlo technique for the solution of state estimation problems, in which the posterior probability density function is represented by a set of random samples (particles) with associated weights. As the number of samples becomes large, the Monte Carlo characterization becomes an equivalent representation of the posterior probability density function and the solution approaches the optimal Bayesian estimate. The Particle Filter algorithms generally make use of an importance density, which is a probability density function proposed to represent another one that cannot be exactly computed, that is, the sought posterior density in the present case. Then, samples are drawn from the importance density instead of the actual density [1–3,12].

For the simultaneous estimation of state variables and nondynamic parameters, let $\{\mathbf{x}_k^i, \boldsymbol{\theta}_k^i\}$ be the particle i at time time t_k, with associated weight w_k^i, $i = 1, \ldots, N$, where N is the number of particles. The subscript k for the parameter vector $\boldsymbol{\theta}$ does not represent a time dependence of such quantity, but the fact is that it is also estimated sequentially, like the state variables $\mathbf{x}$. The weights are normalized so that $\sum_{i=1}^{N} w_k^i = 1$. The posterior probability distribution of the state variables and of the parameters at t_k can be discretely approximated by [6,61]

$$\pi(\mathbf{x}_k, \boldsymbol{\theta}_k|\mathbf{z}_{1:k}) \approx \sum_{i=1}^{N} w_k^i \delta(\mathbf{x}_k - \mathbf{x}_k^i, \boldsymbol{\theta}_k - \boldsymbol{\theta}_k^i) \tag{7}$$

where $\delta(.)$ is the Dirac delta function.

The joint state and parameter estimation problem is a difficult task. For example, an artificial evolution model for the parameters can be used, such as a random walk, but the particles may quite fast loose diversity. The problem is still an active area of research for Particle Filter methods, but the algorithm of Liu and West [4] is considered as a robust and powerful technique [6]. The algorithm of Liu and West for the Particle Filter is based on West's hypothesis [59] of a Gaussian mixture for the vector of parameters $\boldsymbol{\theta}$ [4,63], that is,

$$\pi(\boldsymbol{\theta}|\mathbf{z}_{1:k-1}) \approx \sum_{i=1}^{N} w_{k-1}^{i}\, N(\boldsymbol{\theta}|\mathbf{m}_{k-1}^{i}, h^2\mathbf{V}_{k-1}) \tag{8}$$

where $N(\cdot|\mathbf{m},\mathbf{S})$ is a Gaussian multivariate density with mean $\mathbf{m}$ and covariance matrix $\mathbf{S}$, while h is a smoothing parameter. Equation (8) shows that the density $\pi(\boldsymbol{\theta}|\mathbf{z}_{1:k-1})$ is a mixture of $N(\boldsymbol{\theta}|\mathbf{m}_{k-1}^{i}, h^2\mathbf{V}_{k-1})$ Gaussian distributions weighted by the sample weights w_{k-1}^{i}. The kernel locations are specified by using the following shrinkage rule [4,6]:

$$\mathbf{m}_{k-1}^{i} = A\,\boldsymbol{\theta}_{k-1}^{i} + (1-A)\bar{\boldsymbol{\theta}}_{k-1} \tag{9}$$

where $A=\sqrt{1-h^2}$ and $\bar{\boldsymbol{\theta}}_{k-1}$ is the mean of $\boldsymbol{\theta}$ at time t_{k-1}. The shrinkage factor, A, is computed as [4,6]

$$A = \frac{3\varepsilon - 1}{2\varepsilon} \tag{10}$$

where $0.95 < \varepsilon < 0.99$.

The steps of Liu and West's particle filter algorithm [4,6], as applied for the advancement of the particles from time t_{k-1} to time t_k, are presented in Table 1.

Nonstationary Approximation Error Approach

An implicit assumption made in the state-space model given by Eq. (6) is that both evolution and observation models describe as accurately as possible the physical problem under analysis. The fulfillment of this requirement might be unpractical from a computational point of view and makes the state estimation prohibitive, especially, when complex multiphysical phenomena are involved. An alternative is to use techniques of model reduction to reduce the computational time and then account for the modeling errors in order to avoid poor estimates of the unknown quantities of interest.

The AEM, first proposed for stationary inverse problems [12] and then extended to nonstationary inverse problems [24], is effective for handling the effects of model reduction. The method was successfully applied to compensate for the use of reduced mathematical/computational models in different applications of practical interest, including process monitoring, tomography, and hyperthermia treatment of cancer [11–25,64–66]. In the nonstationary version of the AEM, model reduction error in both evolution and observation models is treated as additional noises. These errors are then modeled as Gaussian and their statistics (means and covariance matrices) are computed based on the probabilistic modeling of the prior information available. In this way, the heavy computational task is performed before the measurements are made.

Let $\mathbf{f}_k^r(\mathbf{x}_k^r,\boldsymbol{\theta}^r,\mathbf{w}_k^r)$ and $\mathbf{g}_k^r(\mathbf{x}_k^r,\boldsymbol{\theta}^r)$ be reduced evolution and observation models, respectively, with parameter vector $\boldsymbol{\theta}^r$ and state vector $\mathbf{x}_k^r$ of dimensions smaller than those of $\boldsymbol{\theta}$ and $\mathbf{x}_k$, respectively, which appear in the accurate models $\mathbf{f}_k(\mathbf{x}_k,\boldsymbol{\theta},\mathbf{w}_k)$ and $\mathbf{g}_k(\mathbf{x}_k,\boldsymbol{\theta})$. For state-space models defined by discrete numerical methods of partial differential equations, a natural choice for reduced models is the use of coarse meshes. Hence, we consider the existence of a linear operator, typically an interpolation mapping P_x between a sufficiently refined mesh and a coarse mesh, so that $\mathbf{x}_k^r = P_x\mathbf{x}_k$ [21–25]. It follows that:

$$\mathbf{x}_k^r = \mathbf{f}_k^r(\mathbf{x}_{k-1}^r,\boldsymbol{\theta}^r,\mathbf{w}_k^r) + \boldsymbol{\omega}_k^r \tag{11}$$

where $\boldsymbol{\omega}_k^r$ represents the modeling error of the process at time t_k and is defined as

$$\boldsymbol{\omega}_k^r = P_x\mathbf{f}_k(\mathbf{x}_{k-1},\boldsymbol{\theta},\mathbf{w}_k) - \mathbf{f}_k^r(\mathbf{x}_{k-1}^r,\boldsymbol{\theta}^r,\mathbf{w}_k^r) \tag{12}$$

Table 1 Liu and West's algorithm [4]

Step 1
Find the mean $\bar{\boldsymbol{\theta}}_{k-1}$ of the parameters $\boldsymbol{\theta}$ at time t_{k-1}
Step 2
For $i=1,\ldots,N$ compute $\mathbf{m}_{k-1}^{i}$ with Eq. (9), draw new particles $\mathbf{x}_k^i$ from the prior density $\pi(\mathbf{x}_k|\mathbf{x}_{k-1}^i,\ \mathbf{m}_{k-1}^i)$ and then calculate the mean $\boldsymbol{\mu}_k^i$ of $\mathbf{x}_k$. Use the likelihood density to calculate the corresponding weights $w_k^i = \pi(\mathbf{z}_k|\boldsymbol{\mu}_k^i,\ \mathbf{m}_{k-1}^i)w_{k-1}^i$
Step 3
Calculate the total weight $t=\sum_i w_k^i$ and then normalize the particle weights, that is, for $i=1,\ldots,N$ let $w_k^i = t^{-1}w_k^i$
Step 4
Resample the particles as follows
Construct the cumulative sum of weights (CSW) by computing $c_i = c_{i-1} + w_k^i$ for $i=1,\ldots,N$, with $c_0=0$
Let $i=1$ and draw a starting point u1 from the uniform distribution $U[0,N^{-1}]$
For $j=1,\ldots,N$
Move along the CSW by making $u_j = \mathrm{u}_1 + N^{-1}(\mathrm{j}-1)$
While $u_j > c_i$ make $i=i+1$
Assign samples $\mathbf{x}_{k-1}^j = \mathbf{x}_{k-1}^i$, $\mathbf{m}_{k-1}^j = \mathbf{m}_{k-1}^i$ and $\boldsymbol{\mu}_k^j = \boldsymbol{\mu}_k^i$
Assign parent $i_j = i$
Step 5
For $j=1,\ldots,$ N draw samples $\boldsymbol{\theta}_k^j$ from $N(\boldsymbol{\theta}_k^j|\mathbf{m}_{k-1}^{ij}, h^2\mathbf{V}_{k-1})$, by using the parent ij
Step 6
For $j=1,\ldots,N$ draw particles $\mathbf{x}_k^j$ from the prior density $\pi(\mathbf{x}_k|\mathbf{x}_{k-1}^{ij},\ \boldsymbol{\theta}_k^j)$, by using the parent ij, and then use the likelihood density to calculate the corresponding weights $w_k^j = \pi(\mathbf{z}_k|\mathbf{x}_k^j,\boldsymbol{\theta}_k^j)/\pi(\mathbf{z}_k|\boldsymbol{\mu}_k^{ij},\mathbf{m}_{k-1}^{ij})$
Step 7
Calculate the total weight $t=\sum_j w_k^j$ and then normalize the particle weights, that is, for $j=1,\ldots,N$ let $w_k^j = t^{-1}w_k^j$

Table 2 Thermophysical and optical properties [48,49,63,67]

Tissue	Epidermis	Tumor	Dermis	Fat	Muscle
Thickness (mm)	0.1	0.75	1.5	2	8
ρ (kg/m^3)	1200	1030	1200	1000	1085
c_p (J/kg K)	3589	3852	3300	2674	3800
k (W/m K)	0.235	0.558	0.445	0.185	0.51
Q_{met} (W/m^3)	0	3680	368.1	368.3	684.2
ω_b (s^{-1})	0	63×10^{-4}	2×10^{-4}	10^{-4}	27×10^{-4}
κ (m^{-1})	35	122	122	108	54
σ_s (m^{-1})	21,270	22,500	22,500	20,200	6670

Table 3 Optical properties of the tumor containing gold nanorods

Concentration of nanoparticles (m^{-3})	3×10^{15}
κ (m^{-1})	177.02
σ_s (m^{-1})	22503.46

Similarly, by assuming that the measurement error is additive, the observation model can be rewritten as [21–25]

$$\mathbf{z}_k = \mathbf{g}_k^r(\mathbf{x}_k^r, \boldsymbol{\theta}^r) + \boldsymbol{\upsilon}_k^r + \mathbf{v}_k \tag{13}$$

where $\boldsymbol{\upsilon}_k^r$ represents the modeling error in the observation model and is given by

$$\boldsymbol{\upsilon}_k^r = \mathbf{g}_k(\mathbf{x}_k, \boldsymbol{\theta}) - \mathbf{g}_k^r(\mathbf{x}_k^r, \boldsymbol{\theta}^r) \tag{14}$$

Therefore, Eq. (13) becomes

$$\mathbf{z}_k = \mathbf{g}_k^r(\mathbf{x}_k^r, \boldsymbol{\theta}^r) + \boldsymbol{\eta}_k, \quad k = 1, 2, \ldots, M \tag{15}$$

where

$$\boldsymbol{\eta}_k = \boldsymbol{\upsilon}_k^r + \mathbf{v}_k \tag{16}$$

Although analytical expressions of the approximation errors can be derived for linear models, in the case of nonlinear models, such as in this work, one shall rely on sampling techniques to obtain the statistics describing the approximation errors [21–25]. The general assumption is that the approximation errors have Gaussian distributions. A Monte Carlo simulation is then performed in order to obtain samples $\boldsymbol{\omega}_k^{r,i}$ and $\boldsymbol{\upsilon}_k^{r,i}$ of the approximation errors. From these samples, one can compute statistics of the approximation errors, such as the means and the covariance matrices, and the reduced evolution-observation models given by Eqs. (11) and (15) can be used in the particle filter computations, instead of the complete models given by Eqs. (6*a*) and (6*b*).

Results and Discussion

For the results presented below, we considered the tissues with thicknesses and physical properties given by Table 2 (see also

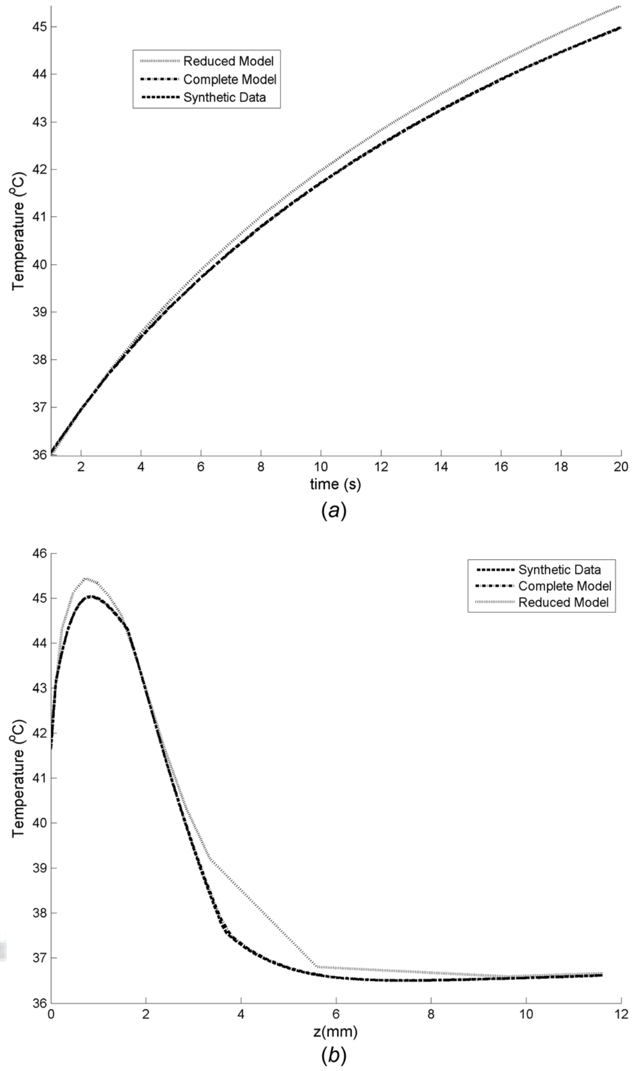

Fig. 2 Comparison of the temperatures obtained with the three different models: (*a*) transient variation at ($r = 0.6$ mm, $z = 0.73$ mm) and (*b*) along the centerline at $t = 20$ s

Fig. 1) [50,51,68]. Absorption and scattering coefficients of the tumor loaded with gold nanorods are shown in Table 3 and were computed following the procedure given in Ref. [40], by assuming a volumetric concentration $3\times10^{15}\,\text{m}^{-3}$ of nanorods, with peak surface plasmon resonance at $\lambda_{\text{SPR}} = 798$ nm and aspect ratio $R = 3.9$ [69]. The remaining physical properties were assumed as not affected by the inclusion of the nanoparticles. The first and second moments of Fresnel reflection coefficient for the air–tissue interface, with the tissue refractive index of 1.3, are given by 0.565 and 0.429, respectively [70]. The steady-state version of the bioheat transfer problem given by Eq. (5) was solved in order to obtain the initial distribution of temperature in the skin model, with $Q_{\text{laser}}(r,z) = 0$, $h_c = 10\,\text{W/m}^2\,\text{K}$ and $h_{\text{int}} = 50\,\text{W/m}^2\,\text{K}$ [40]. AQ5

The subcutaneous tumor that is the target of the hyperthermia treatment was assumed loaded with gold nanorods and then

Table 4 Finite volume meshes

Mesh	Number of control volumes in the radial direction	Number of control volumes in the axial direction	Total number of control volumes	Purpose
$\mathcal{M}_1$	10	15	150	Reduced model
$\mathcal{M}_2$	100	150	15,000	Complete model
$\mathcal{M}_3$	200	300	60,000	Synthetic data

Table 5 Prior probability densities for the optical parameters

Optical parameter	Mean	Standard deviation
Absorption coefficient	κ_0	$0.05\kappa_0/2.576$
Scattering coefficient	$\sigma_{s,0}$	$0.05\sigma_{s,0}/2.576$
Anisotropy factor	g_0	$0.03g_0/2.576$
Fresnel's parameter	$A_{1,0}$	$0.001A_{1,0}/2.576$
Specular reflectivity	R_s	$0.01R_{s,0}/2.576$
Irradiance	E_0	$0.05\,E_0/2.576$

Table 6 Prior probability densities for the thermophysical parameters

Parameter	Mean	Standard deviation
Thermal conductivity	k_0	$0.05\,k_{,0}/2.576$
Volumetric heat capacity	$c_{p,0}$	$0.05c_{p,0}/2.576$
Perfusion coefficient	ω_0	$0.05\,\omega_0/2.576$
Metabolic heat source	$Q_{\mathrm{met},0}$	$0.05\,Q_{\mathrm{met},0}/2.576$
Heat transfer coefficients	$h_{c,0}$ $h_{\mathrm{int},0}$	$0.05h_{c,0}/2.576$ $0.05h_{\mathrm{int},0}/2.576$

exposed to a collimated uniform laser beam ($\lambda = 800$ nm, $E_0 = 1.2\ \mathrm{W/cm^2}$) during 20 s under CW. A heat transfer coefficient $h_c = 500\ \mathrm{W/m^2\ K}$ to a medium at $T_c = 35\,^\circ\mathrm{C}$ was considered for radial positions smaller than the tumor radius in order to simulate the effect of an active cooling mechanism at the skin surface [40,41,57]. The heat transfer coefficient for larger radial positions was set to $h_c = 10\ \mathrm{W/m^2\ K}$ [40].

Both radiation and bioheat transfer problems were numerically solved using a finite volume code based on the alternating direction implicit method. The code was verified against analytical solutions for limiting cases. The coupled radiation-bioheat transfer problem defined by Eqs. (1) and (5) was solved with three different finite volume meshes, referred to as $\mathcal{M}_1$, $\mathcal{M}_2$, and $\mathcal{M}_3$, with the number of volumes shown by Table 4. The most refined mesh, $\mathcal{M}_3$, was used for the generation of the simulated measurements, in order to avoid an inverse crime. Meshes $\mathcal{M}_1$ and $\mathcal{M}_2$ were used for the solution of the state estimation problem with the reduced and complete models, respectively. Figure 2(*a*) presents the comparison of the transient temperature variation at the position ($r = 0.6$ mm, $z = 0.73$ mm) obtained using these three different meshes for the solution of the coupled radiation-bioheat transfer problem. Similarly, Fig. 2(*b*) presents the temperature distributions obtained with these same meshes in the axial direction along the centerline, at $t = 20$ s. One can notice in these figures discrepancies between the temperature profiles obtained with the complete and reduced models. These discrepancies are due to the

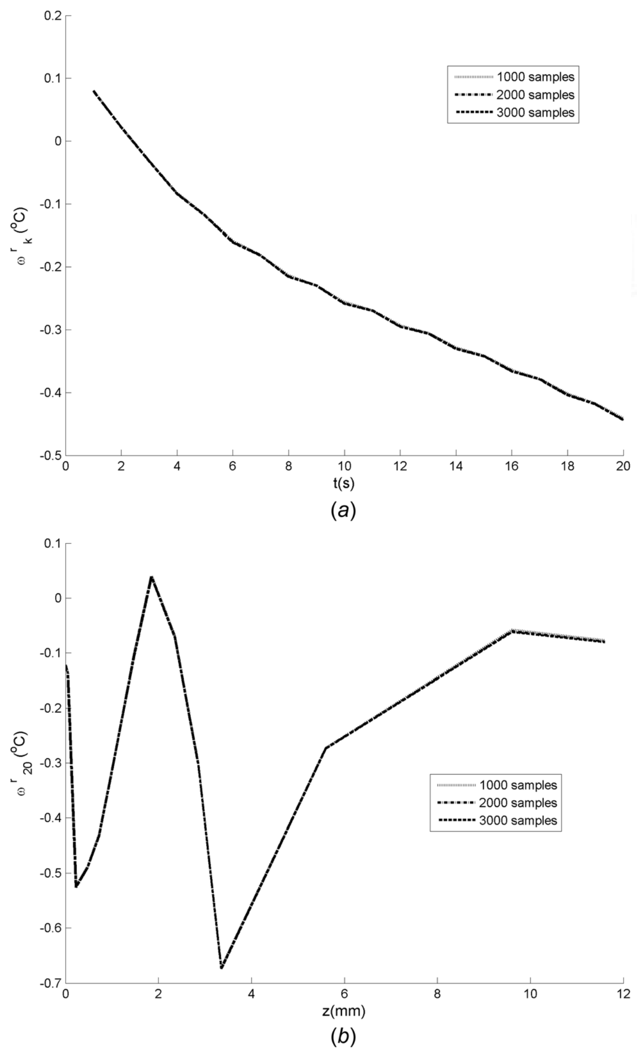

Fig. 3 Convergence of the mean of the approximation error: (*a*) transient variation at ($r = 0.6$ mm, $z = 0.73$ mm) and (*b*) along the centerline at $t = 20$ s

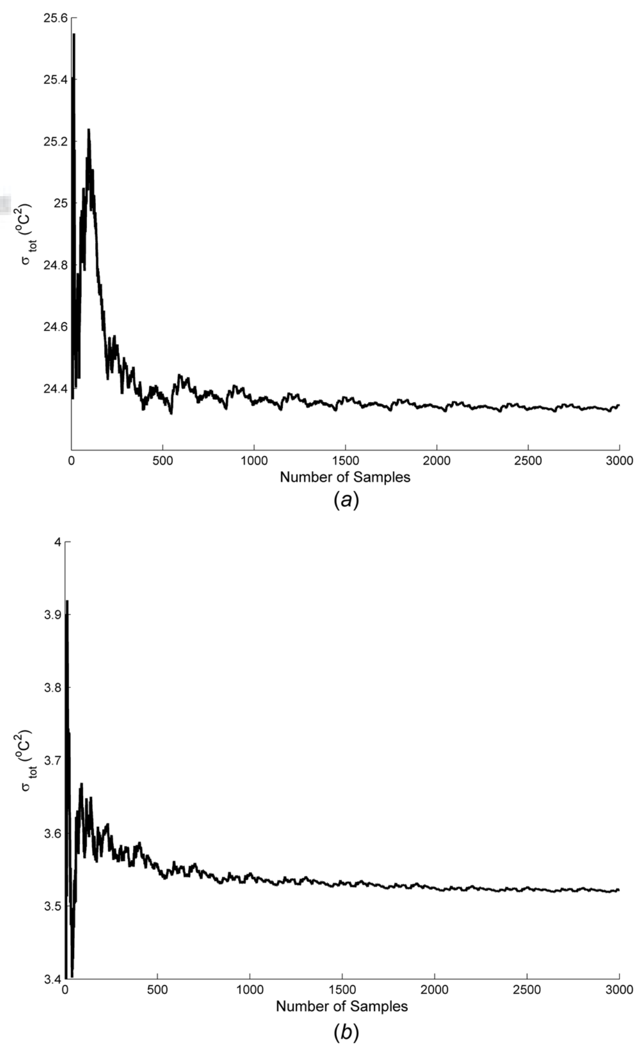

Fig. 4 Convergence of the total sample variance of the approximation error: (*a*) at $t = 1$ s and (*b*) at $t = 20$ s

use of the nonconverged finite volume mesh M_1. On the other hand, one can note that the mesh M_2 is sufficiently refined, since the solution of the complete model graphically matches the solution obtained with mesh M_3, which was used to generate the synthetic measured data. The results obtained with mesh M_3 will be considered as exact for the comparisons performed hereafter.

The statistics of the approximation error between the reduced model (mesh M_1) and the complete model (mesh M_2) were computed with a Monte Carlo simulation by assuming the prior probability densities given by Tables 5 and 6 for the physical parameters in the vector $\boldsymbol{\theta}$, where the reference values (subscript 0) are given by Tables 2 and 3. These prior densities are based on literature data [48,49,63,67]. For the Monte Carlo simulation, the complete state evolution model was assumed as deterministic. For the calculation of the statistics of the approximation error $\boldsymbol{\omega}_k^r$, 3000 samples were generated from the prior probability densities given by Tables 5 and 6. The convergence of the statistics of the approximation error is presented by Figs. 3 and 4. Figures 3(*a*) and 3(*b*) present the means of the errors at ($r = 0.6$ mm, $z = 0.7$ mm) and along the axial direction at $r = 0$ mm and $t = 20$ s, respectively, for different number of samples used in the Monte Carlo simulation. Figures 4(*a*) and 4(*b*) present the variation of the trace of the covariance matrix of the approximation error with the number of samples, at $t = 1$ s and $t = 20$ s, respectively. Figures

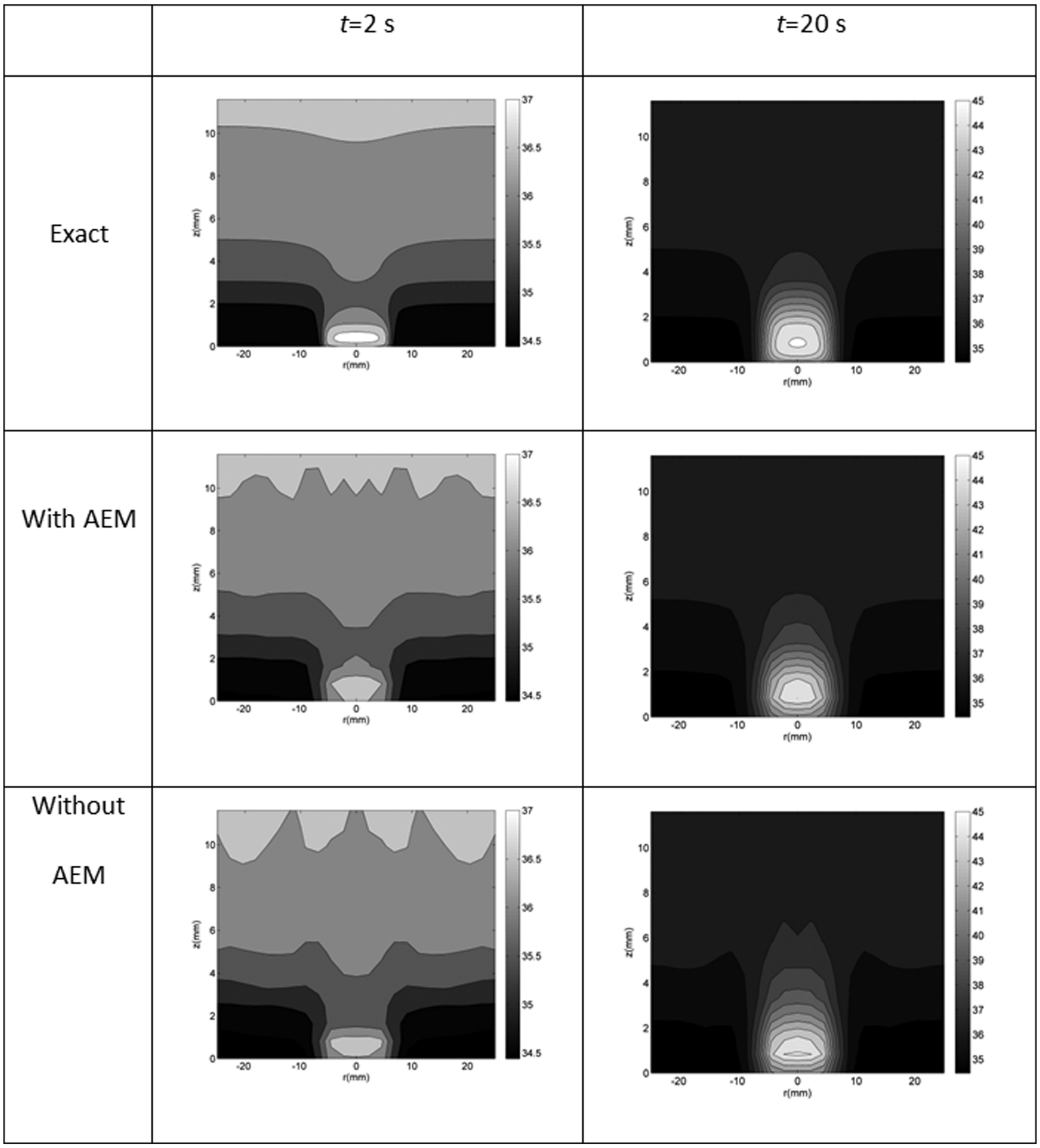

Fig. 5 Exact and estimated temperature distribution at selected times with $N = 250$ particles

3 and 4 show that convergence is achieved for the means and covariance matrices of the approximation error with the number of samples utilized.

Once the statistics of the approximation error are computed, the solution of the state estimation problem can be obtained with the computationally fast reduced model, instead of the complete model. For the reduced model, the uncertainties were assumed as additive, that is,

$$\mathbf{x}^r_{k+1} = \mathbf{f}^r_{k+1}(\mathbf{x}^r_k, \boldsymbol{\theta}^r_k) + \boldsymbol{\varepsilon}^r_{k+1} \tag{17a}$$

The evolution model is represented separately for the fluence rate, $\boldsymbol{\Phi}_k$, and temperature, $\mathbf{T}_k$, as

$$\begin{cases} \boldsymbol{\Phi}^r_{k+1} = \boldsymbol{\Phi}^r_k(\boldsymbol{\theta}_k) + \sigma_\Phi \boldsymbol{\varepsilon}^\Phi_{k+1} \\ \mathbf{T}^r_{k+1} = \mathbf{F}^r_{k+1}(\mathbf{T}^r_k, \boldsymbol{\Phi}^r_{k+1}, \boldsymbol{\theta}_k) + \boldsymbol{\omega}^r_{k+1} \end{cases} \tag{17b}$$

In Eq. (17*b*), the evolution model for the fluence rate was defined in the form of a random walk, with uncorrelated and Gaussian noise, with zero mean and a standard deviation $\sigma_\Phi = 1\%$ of its deterministic value. The deterministic values for the fluence rate were obtained from the finite volume solution of problem (1) with mesh M_1. The evolution model for temperature was obtained from the finite volume solution for problem (5) (operator $\mathbf{F}^r_{k+1}$ in Eq. (17*b*)) with mesh M_1, and contains uncertainties given by the approximation error $\boldsymbol{\omega}^r_k$. The uncertainties in the initial temperature distribution are Gaussian, with zero mean and a standard deviation of 0.5 °C.

Transient temperature measurements ($\mathbf{z}^{\mathrm{meas}}_k$) taken at the position ($r = 0.6$ mm, $z = 0.7$ mm), at a rate of one measurement every 1 s, are assumed available for the analysis. The measurement errors are supposed additive, Gaussian, uncorrelated, with zero mean and a constant standard deviation $\sigma_{T_{\mathrm{meas}}} = 0.5$ °C so that the likelihood function written in terms of the reduced model is given by

$$\pi\left(\mathbf{z}^{\mathrm{meas}}_k | \mathbf{x}^r_k, \boldsymbol{\theta}^r\right) \propto \exp\left\{-\frac{1}{2}\left[\mathbf{z}^{\mathrm{meas}}_k - \mathbf{g}^r_k\left(\mathbf{x}^r_k, \boldsymbol{\theta}^r\right) - \bar{\boldsymbol{\eta}}_k\right]^{\mathrm{T}} \mathbf{W}^{-1}_\eta \left[\mathbf{z}^{\mathrm{meas}}_k - \mathbf{g}^r_k\left(\mathbf{x}^r_k, \boldsymbol{\theta}^r\right) - \bar{\boldsymbol{\eta}}_k\right]\right\} \tag{18}$$

where $\bar{\boldsymbol{\eta}}_k$ and $\mathbf{W}_\eta$ are the mean and the covariance matrix of $\boldsymbol{\eta}_k$, respectively, which include the statistics of the approximation errors and of the measurement errors (see Eq. (16)). Since the measurement errors have zero mean and constant standard deviation $\sigma_{T_{\mathrm{meas}}}$, we can write [11]

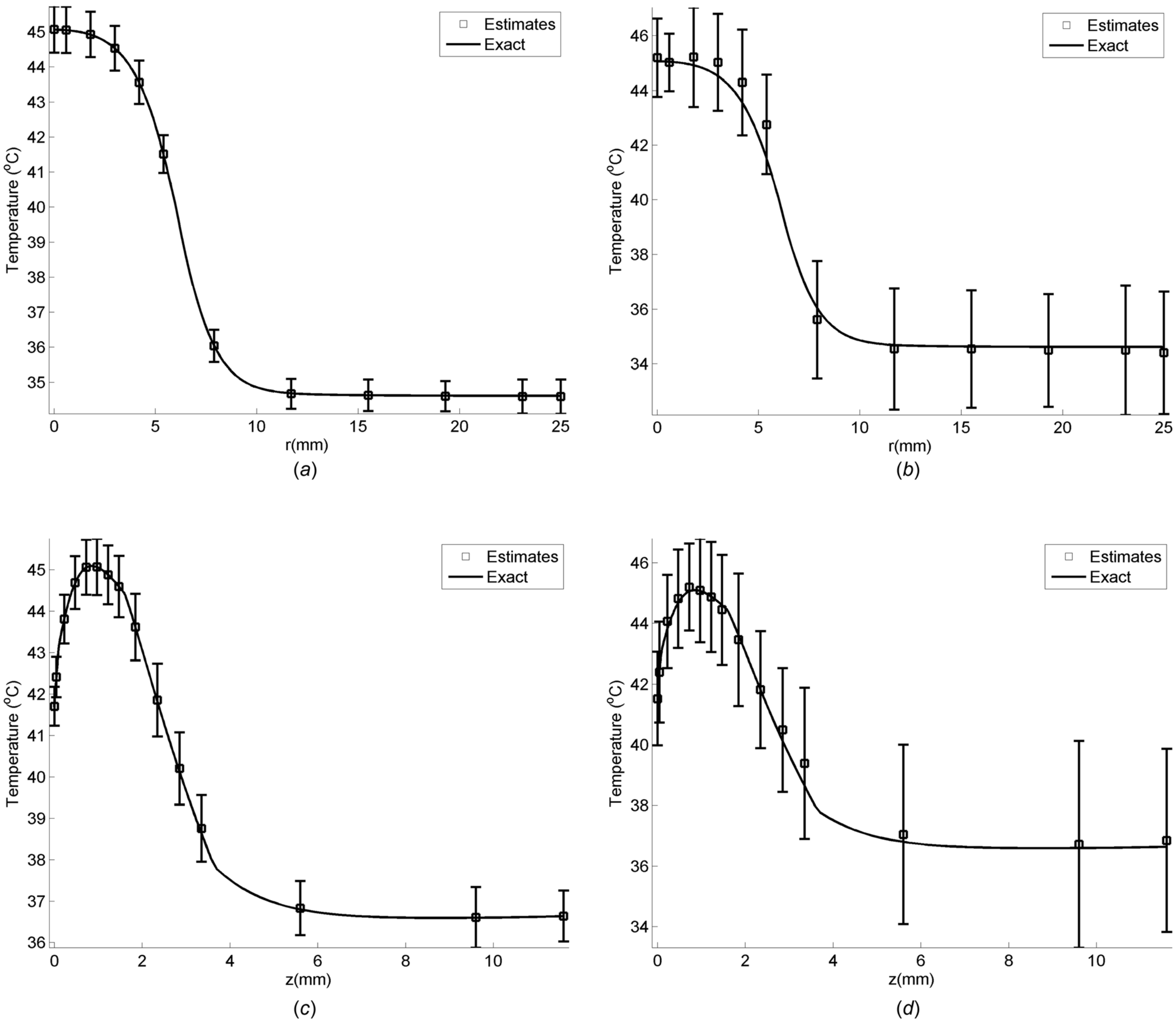

Fig. 6 Estimated and exact temperature distribution at $t = 20$ s: (left) along the radius for a line at $z = 0.7$ mm, with Liu and West and AEM (*a*), Liu and West without AEM (*b*); (right) along the centerline, with Liu and West and AEM (*c*), Liu and West without AEM (*d*)

$$\bar{\boldsymbol{\eta}}_k = \bar{\boldsymbol{v}}_k^r \tag{19a}$$

$$\mathbf{W}_\eta = \mathbf{W}_{v_k^r} + \sigma^2_{T_{\text{meas}}}\mathbf{I} \tag{19b}$$

where $\bar{\boldsymbol{v}}_k^r$ and $\mathbf{W}_{v_k^r}$ are, respectively, the mean and the covariance matrix of approximation error $\boldsymbol{v}_k^r$, while $\mathbf{I}$ is the identity matrix.

Figure 5 presents the estimated temperature distributions obtained with the Liu and West particle filter at selected time instants, for $N = 250$ particles, by using the reduced model together with the AEM. The solution obtained by the simple reduction of the model (without the AEM) is also shown in this figure, as well as the exact temperatures (obtained with the most refined mesh M_3). Figure 5 shows that good estimates of the temperature distributions were obtained when the AEM approach was taken into account. On the other hand, if the AEM is not considered, the agreement between estimated and measured temperatures deteriorates. Such fact is also apparent from the analysis of Figs. 6(*a*)–6(*d*), where the estimated temperature distributions are shown along the radial direction for a line at $z = 0.7$ mm and along the axial direction at the centerline.

For further assessment of the accuracy of the results obtained with the Liu and West algorithm together with the AEM approach, the estimated transient variations of the temperatures at the measurement point, and at a position where no measurements are available ($r = 5.4$ mm, $z = 0.7$ mm), are shown in Figs. 7 and 8, respectively. For comparison, the exact temperatures are shown in these two figures and the simulated temperature measurements are included in Fig. 7. One can notice in Figs. 7 and 8 that excellent estimates were obtained with small credible bounds if the AEM was used. It is interesting to note in Fig. 7(*b*) that the transient temperature variation estimated by the particle filter without the AEM follows the noisy measurements and not the exact temperatures. Furthermore, for a position where no measurements are available, as shown by Fig. 8(*b*), the estimated temperatures do not follow the exact ones and increase at a larger rate. Figures 5–8 demonstrate the sensitivity of the inverse problem solution to modeling errors and also show the importance of compensating for the effects of model reduction by using the AEM.

Liu and West's algorithm for the particle filter allows for simultaneous estimation of the state variables and of the nondynamic model parameters. Selected estimated parameters with their associated 99% credible intervals are presented in Fig. 9. The exact values of these parameters were also included in this figure for the sake of comparison. We note in Fig. 9 that excellent estimates were obtained for the parameters, with the exact values falling inside the credible intervals. Moreover, one can observe a reduction of the credible intervals for some parameters as time

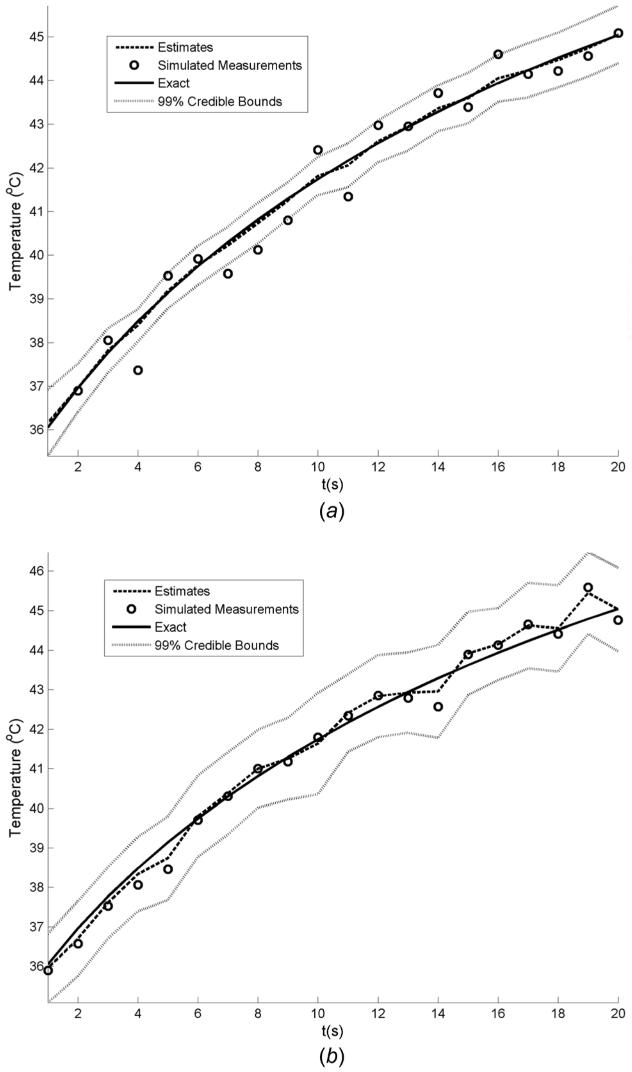

Fig. 7 Comparison of the estimated and exact transient temperature variations with the temperature measurements at the sensor position ($r = 0.6$ mm, $z = 0.7$ mm): (*a*) Liu and West with AEM; (*b*) Liu and West without AEM

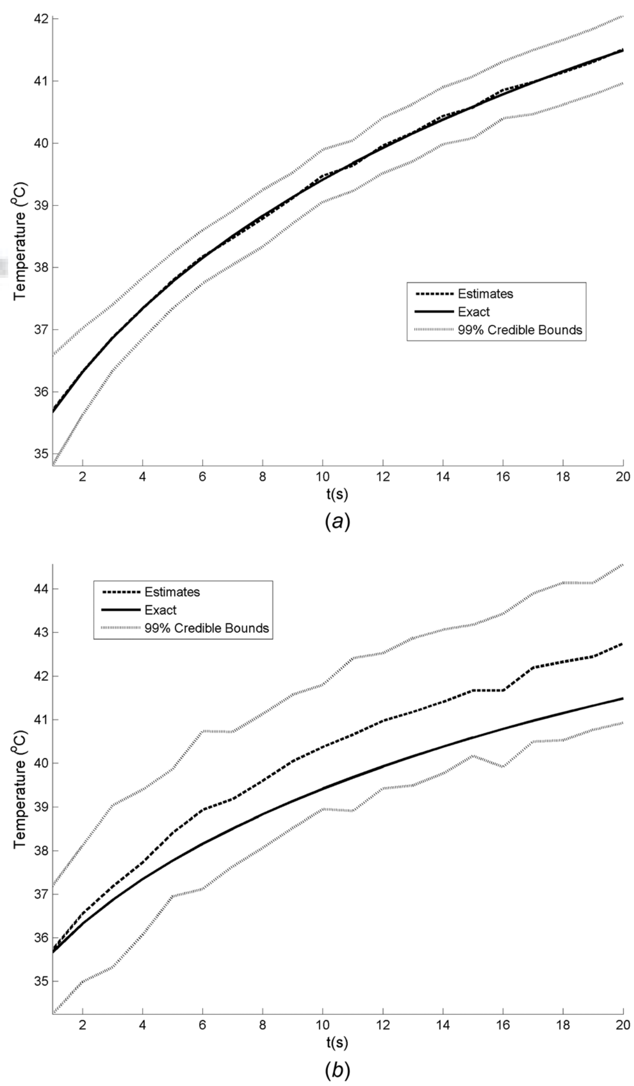

Fig. 8 Estimated and exact transient temperature variations at ($r = 5.4$ mm, $z = 0.7$ mm): (*a*) Liu and West with AEM; (*b*) Liu and West without AEM

increases. Thus, the samples of the corresponding marginal posteriors tend to concentrate around the corresponding exact values as time evolves because of the accumulated information provided by the transient measurements and by the evolution model.

The computational cost for the solution of the simultaneous estimation of parameters and state variables using the complete model was of 81 hrs, with 250 particles [29]. On the other hand, with the reduced model, the solution was obtained in 47 min, which represents a speedup of 100 times. Computational times

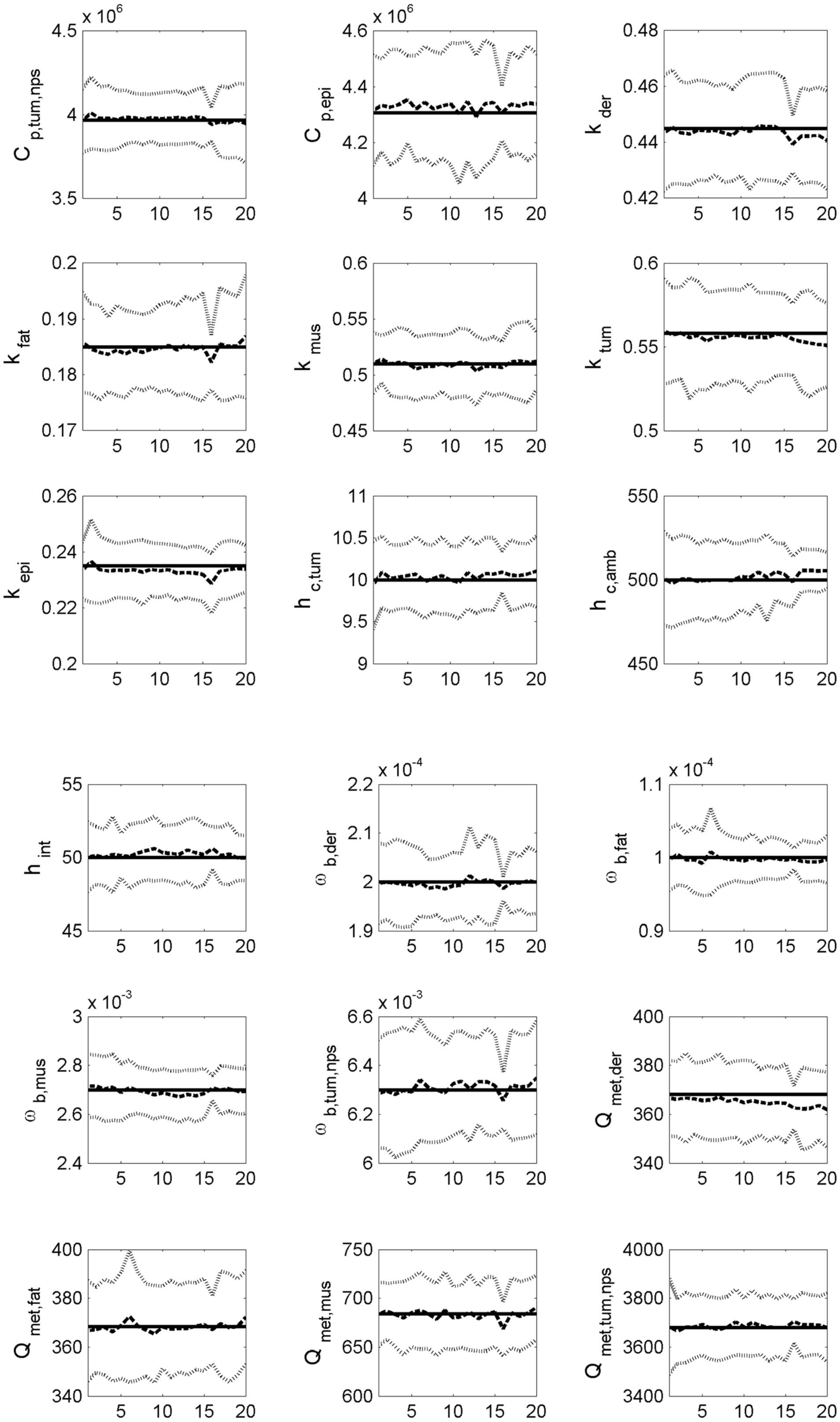

Fig. 9 Estimation of selected parameters (subscripts: tum = tumor, tum, nps = tumor with nanoparticles, epi = epidermis, der = dermis, mus = muscle, amb = surrounding ambient)

refer to codes run under the MATLAB platform, on an Intel(R) Xeon E56445 at 2.40 GHz dual processor with 32 GB of RAM memory.

Conclusions

This work dealt with the solution of a state estimation problem involving the laser heating of a subcutaneous tumor loaded with nanoparticles. A reduced order model, based on the use of a coarse mesh for the solution of the coupled radiation-bioheat transfer problem, was proposed to speed up the solution of the state estimation problem. The AEM was jointly used with the Liu and West Particle Filter algorithm for the simultaneous estimation of state variables and model parameters. Results obtained with simulated measurements show that the present approach provides excellent results for the estimated quantities. It was also demonstrated that, when the model reduction errors were not accounted for, the estimated quantities were not accurate. Furthermore, the use of the reduced model allowed for large reduction of computational times for the solution of the present state estimation problem.

Acknowledgment

The financial support provided by FAPERJ, CAPES, and CNPq, Brazilian agencies for the fostering of science, is greatly appreciated. The authors also acknowledge the support provided by the STIC AmSud project "I3PE—Inverse Problems in Physical Properties Estimation."

Nomenclature

c_p = specific heat
D = diffusion coefficient for the δ-P1 approximation
E_0 = maximum laser radiation flux imposed at $z=0$
g = anisotropy scattering factor
h = heat transfer coefficient
k = thermal conductivity
L_r, L_z = radius and thickness of the cylinder, respectively
N = number of particles for the particle filter
Q = volumetric heat source
r,z = cylindrical coordinates
R_{sc} = specular reflection coefficient at $z=0$
R_1, R_2 = first and second moments of Fresnel's reflection coefficient, respectively
$\hat{\mathbf{s}}_c$ = direction of propagation of the collimated laser beam
t = time
T = temperature
T_s = initial temperature
w = weights
$\mathbf{x}$ = state vector
$\mathbf{z}$ = vector of measurements

Greek Symbols

β_{tr} = transport attenuation coefficient
β_i' = reduced total attenuation coefficient of layer i
$\boldsymbol{\theta}$ = vector containing nondynamic parameters of the model
κ = absorption coefficient
$\pi(a|b)$ = conditional probability of a when b is given
ρ = density
σ_s = scattering coefficient
σ_s' = reduced scattering coefficient
Φ = total fluence rate
Φ_p = collimated component of the fluence rate
Φ_s = diffusive fluence rate
ω_b = blood perfusion rate

Subscripts

b = blood
c = cooling
int = deeper internal tissues
k = time instant t_k
met = metabolism

Superscript

i = particle index

References

[1] Arulampalam, M. S., Maskell, S., Gordon, N., and Clapp, T., 2002, "A Tutorial on Particle Filters for Online Nonlinear/Non-Gaussian Bayesian Tracking," IEEE Trans. Signal Process., **50**(2), pp. 174–188.
[2] Ristic, B., Arulampalam, S., and Gordon, N., 2004, *Beyond the Kalman Filter*, Artech House, Boston, MA.
[3] Doucet, A., de Freitas, N., and Gordon, N., 2001, *Sequential Monte Carlo Methods in Practice*, Springer, New York.
[4] Liu, J., and West, M., 2001, "Combined Parameter and State Estimation in Simulation-Based Filtering," *Sequential Monte Carlo Methods in Practice*, A. Doucet, N. de Freitas, and N. Gordon, eds., Springer, New York.
[5] Sheinson, D. M., Niemi, J., and Meiring, W., 2014, "Comparison of the Performance of Particle Filter Algorithms Applied to Tracking of a Disease Epidemic," Math. Biosci., **255**(■), pp. 21–32.
[6] Lopes, H. F., and Carvalho, C. M., 2013, "Online Bayesian Learning in Dynamic Models: An Illustrative Introduction to Particle Methods," *Bayesian Theory and Applications*, P. Damien, P. Dellaportas, N. G. Polson, and D. A. Stephens, eds., Oxford Press University, ■. AQ6
[7] Smal, I., Niessen, W. J., Demirel, O., Meijering, E., and Sbalzarini, I. F., 2014, "PPF: A Parallel Particle Filtering Library," IET Conference on Data Fusion and Target Tracking 2014: Algorithms and Applications, ■. AQ7
[8] Chitchian, M., Simonetto, A., van Amesfoort, A. S., and Keviczky, T., 2013, "Distributed Computation Particle Filters on GPU Architectures for Real-Time Control Applications," IEEE Trans. Control Syst. Technol., **21**(6), pp. 2224–2238.
[9] Goodrum, M. A., Trotter, M. J., Aksel, A., Acton, S. T., and Skadron, K., 2012, "Parallelization of Particle Filter Algorithms," *Computer Architecture* (Lecture Notes in Computer Science (Including Subseries Lecture Notes in Artificial Intelligence and Lecture Notes in Bioinformatics)), Vol. 6161, ■, ■, pp. 139–149. AQ8
[10] Brown, J. A., and Capson, D. W., 2012, "A Framework for 3D Model-Based Visual Tracking Using a GPU-Accelerated Particle Filter," IEEE Trans. Visualization Comput. Graphics, **18**(1), pp. 68–80.
[11] Lamien, B., Orlande, H. R. B., Eliçabe, G. E., and Maurente, A. J., 2014, "State Estimation Problem in Hyperthermia Treatment of Tumors Loaded With Nanoparticles," 15th International Heat Transfer Conference, Kyoto, Japan, pp. 1–15.
[12] Kaipio, J. P., and Somersalo, E., 2004, *Statistical and Computational Inverse Problems* (Applied Mathematical Sciences) Vol. 160, Springer-Verlag, ■.
[13] Kaipio, J. P., and Somersalo, E., 2007, "Statistical Inverse Problems: Discretization, Model Reduction and Inverse Crimes," J. Comput. Appl. Math., **198**(2), pp. 493–504.
[14] Nissinen, A., Heikkinen, L. M., and Kaipio, J. P., 2008, "The Bayesian Approximation Error Approach for Electrical Impedance Tomography—Experimental Results," Meas. Sci. Technol., **19**(1), p. 015501.
[15] Nissinen, A., Heikkinen, L. M., Kolehmainen, V., and Kaipio, J. P., 2009, "Compensation of Errors Due to Discretization, Domain Truncation and Unknown Contact Impedances in Electrical Impedance Tomography," Meas. Sci. Technol., **20**(10), p. 105504.
[16] Nissinen, A., ■, "Modelling Errors in Electrical Impedance Tomography," Ph.D. thesis, ■, ■. AQ9
[17] Nissinen, A., Kolehmainen, V. P., and Kaipio, J. P., 2011, "Compensation of Modelling Errors Due to Unknown Domain Boundary in Electrical Impedance Tomography," IEEE Trans. Med. Imaging, **30**(2), pp. 231–242.
[18] Mozumder, M., Tarvainen, T., Kaipio, J. P., Arridge, S. R., and Kolehmainen, V., 2014, "Compensation of Modeling Errors Due to Unknown Domain Boundary in Diffuse Optical Tomography," J. Opt. Soc. Am. A, **31**(8), pp. 1847–1855.
[19] Tarvainen, T., Kolehmainen, V., Pulkkinen, A., Vauhkonen, M., Schweiger, M., Arridge, S. R., and Kaipio, J. P., 2010, "An Approximation Error Approach for Compensating for Modelling Errors Between the Radiative Transfer Equation and the Diffusion Approximation in Diffuse Optical Tomography," Inverse Probl., **26**(1), p. 015005.
[20] Kolehmainen, V., Tarvainen, T., Arridge, S. R., and Kaipio, J. P., 2011, "Marginalization of Uninteresting Distributed Parameters in Inverse Problems—Application to Diffuse Optical Tomography," Int. J. Uncertainty Quantif., **1**(1), pp. 1–17.
[21] Huttunen, J. M. J., and Kaipio, J. P., 2007, "Approximation Error Analysis in Nonlinear State Estimation With an Application to State-Space Identification," Inverse Probl., **23**(5), pp. 2141–2157.
[22] Huttunen, J. M. J., Lehikoinen, A., Hämäläinen, J., and Kaipio, J. P., 2010, "Importance Sampling Approach for the Nonstationary Approximation Error Method," Inverse Probl., **26**(12), p. 125003.
[23] Huttunen, J. M. J., and Pikkarainen, H. K., 2007, "Discretization Error in Dynamical Inverse Problems: One-Dimensional Model Case," J. Inverse Ill-Posed Probl., **15**(4), pp. 365–386. AQ15

[24] Huttunen, J., and Kaipio, J. P., 2007, "Approximation Errors in Nonstationary Inverse Problems," Inverse Probl. Imaging, **1**(1), pp. 77–93.

[25] Huttunen, J. M. J., and Kaipio, J. P., 2009, "Model Reduction in State Identification Problems With an Application to Determination of Thermal Parameters," Appl. Numer. Math., **59**(5), pp. 877–890.

[26] Lamien, B., Orlande, H. R. B., and Eliçabe, G. E., 2015, "Comparison of Particle Filter Algorithms Applied to the Temperature Filed Estimation in Hyperthermia Phantoms," 1st Thermal and Fluid Engineering Summer Conference, ASTFE, New York, Paper No. TFESC–13764. AQ10

[27] Lamien, B., Orlande, H. R. B., and Eliçabe, G. E., 2015, "Inverse Problem in the Hyperthermia Therapy of Cancer With Laser Heating and Plasmonic Nanoparticles," Inverse Probl. Sci. Eng., ■(■), pp. ■–■. AQ11

[28] Varon, L. A. B., Orlande, H. R. B., and Elicabe, G., 2016, "Combined Parameter and State in the Radiofrequency Hyperthermia Treatment of Cancer," Numer. Heat Transfer, Part A (in press). AQ12

[29] Lamien, B., Varon, L. A. B., Orlande, H. R. B., and Eliçabe, G. E., 2016, "State Estimation in Bioheat Transfer: A Comparison of Particle Filter Algorithms," Int. J. Numer. Methods Heat Fluid Flow (in press).

[30] Varon, L. A. B., Orlande, H. R. B., and Elicabe, G., 2015, "Estimation of State Variables in the Hyperthermia Therapy of Cancer With Heating Imposed by Radiofrequency Electromagnetic Waves," Int. J. Therm. Sci., **98**(■), pp. 228–236.

[31] dos Santos, I., Haemmerich, D., Schutt, D., da Rocha, A. F., and Menezes, L. R., 2009, "Probabilistic Finite Element Analysis of Radiofrequency Liver Ablation Using the Unscented Transform," Phys. Med. Biol., **54**(3), pp. 627–640.

[32] de Greef, M., Kok, H. P., Correia, D., Borsboom, P. P., Bel, A., and Crezee, J., 2011, "Uncertainty in Hyperthermia Treatment Planning: The Need for Robust System Design," Phys. Med. Biol., **56**(11), pp. 3233–3250.

[33] Liu, J., 2001, "Uncertainty Analysis for Temperature Prediction of Biological Bodies Subject to Randomly Spatial Heating," J. Biomech., **34**(12), pp. 1637–1642.

[34] Liu, J., 2014, "Ways Toward Targeted Freezing or Heating Ablation of Malignant Tumor: Precisely Managing the Heat," 15th International Heat Transfer Conference, IHTC-15, Kyoto, Japan, pp. 1–25.

[35] Xu, X., Meade, A., and Bayazitoglu, Y., 2011, "Numerical Investigation of Nanoparticle-Assisted Laser-Induced Interstitial Thermotherapy Toward Tumor and Cancer Treatments," Lasers Med. Sci., **26**(2), pp. 213–222.

[36] Tjahjono, I. K., and Bayazitoglu, Y., 2008, "Near-Infrared Light Heating of a Slab by Embedded Nanoparticles," Int. J. Heat Mass Transfer, **51**(■), pp. 1505–1515.

[37] Vera, J., and Bayazitoglu, Y., 2009, "A Note on Laser Penetration in Nanoshell Deposited Tissue," Int. J. Heat Mass Transfer, **52**(■), pp. 3402–3406.

[38] Vera, J., and Bayazitoglu, Y., 2009, "Gold Nanoshell Density Variation With Laser Power for Induced Hyperthermia," Int. J. Heat Mass Transfer, **52**(■), pp. 564–573.

[39] Bayazitoglu, Y., Kheradmand, S., and Tullius, T. K., 2013, "An Overview of Nanoparticle Assisted Laser Therapy," Int. J. Heat Mass Transfer, **67**(■), pp. 469–486.

[40] Dombrovsky, L. A., Timchenko, V., and Jackson, M., 2012, "Indirect Heating Strategy for Laser Induced Hyperthermia: An Advanced Thermal Model," Int. J. Heat Mass Transfer, **55**(■), pp. 4688–4700.

[41] Dombrovsky, L. A., Timchenko, V., Jackson, M., and Yeoh, G. H., 2011, "A Combined Transient Thermal Model for Laser Hyperthermia of Tumors With Embedded Gold Nanoshells," Int. J. Heat Mass Transfer, **54**(■), pp. 5459–5469.

[42] Chatterjee, D., and Krishnan, S., 2013, "Gold Nanoparticle—Mediated Hyperthermia in Cancer Therapy," *Cancer Nanotechnology: Principles and Applications in Radiation Oncology*, S. Cho, and S. Krishnan, eds., CRC Press, Boca Raton, FL.

[43] van der Zee, J., 2002, "Heating the Patient: A Promising Approach?," Ann. Oncol., **13**(8), pp. 1173–1184.

[44] Tamarov, K. P., Osminkina, L. A., Zinovyev, S. V., Maximova, K. A., Kargina, J. V., Gongalsky, M. B., Ryabchikov, Y., et al., 2014, "Radio Frequency Radiation-Induced Hyperthermia Using Si Nanoparticle-Based Sensitizers for Mild Cancer Therapy," Sci. Rep., **4**(■), p. 7034. AQ13

[45] Wang, Q., Xie, L., He, Z., Di, D., and Liu, J., 2012, "Biodegradable Magnesium Nanoparticle-Enhanced Laser Hyperthermia Therapy," Int. J. Nanomed., **7**(■), pp. 4715–4725.

[46] Rengan, A. K., Bukhari, A. B., Pradhan, A., Malhotra, R., Banerjee, R., Srivastava, R., and De, A., 2015, "In Vivo Analysis of Biodegradable Liposome Gold Nanoparticles as Efficient Agents for Photothermal Therapy of Cancer," Nano Lett., **15**(2), pp. 842–848.

[47] Pearce, J. A., 2013, "Comparative Analysis of Mathematical Models of Cell Death and Thermal Damage Processes," Int. J. Hyperthermia, **29**(4), pp. 262–280.

[48] van Rhoon, G. C., 2016, "Is CEM43 Still a Relevant Thermal Dose Parameter for Hyperthermia Treatment Monitoring?," Int. J. Hyperthermia, **32**(1), pp. 50–62.

[49] Clinicaltrials, 2010, "Pilot Study of AuroLase(tm) Therapy in Refractory and/or Recurrent Tumors of the Head and Neck," National Institutes of Health, ■.

[50] Çetingül, M. P., and Herman, C., 2010, "A Heat Transfer Model of Skin Tissue for the Detection of Lesions: Sensitivity Analysis," Phys. Med. Biol., **55**(19), pp. 5933–5951.

[51] Çetingül, M. P., and Herman, C., 2011, "Quantification of the Thermal Signature of a Melanoma Lesion," Int. J. Therm. Sci., **50**(4), pp. 421–431.

[52] Star, W. M., 2011, "Diffusion Theory of Light Transport," *Optical-Thermal Response of Laser-Irradiated Tissue*, A. J. Welch, and M. J. C. van Gemert, eds., Springer, New York.

[53] Carp, S. A., Prahl, S. A., and Venugopalan, V., 2004, "Radiative Transport in the Delta-P1 Approximation: Accuracy of Fluence Rate and Optical Penetration Depth Predictions in Turbid Semi-Infinite Media," J. Biomed. Opt., **9**(3), pp. 632–647.

[54] Elliott, A. M., Stafford, R. J., Schwartz, J., Wang, J., et al., 2007, "Laser-Induced Thermal Response and Characterization of Nanoparticles for Cancer Treatment Using Magnetic Thermal Imaging," Med. Phys. J., **34**(7), pp. 3102–3108.

[55] Dombrovsky, L. A., Randrianalisoa, J. H., Lipinski, W., and Timchenko, V., 2013, "Simplified Approaches to Radiative Transfer Simulations in Laser-Induced Hyperthermia of Superficial Tumors," Comput. Therm. Sci., **5**(6), pp. 521–530.

[56] Pennes, H. H., 1948, "Analysis of Tissue and Arterial Blood Temperatures in the Resting Human Forearm," J. Appl. Physiol., **1**(2), pp. 93–122.

[57] Singh, R., Das, K., Okajima, J., Maruyama, S., and Mishra, S. C., 2015, "Modeling Skin Cooling Using Optical Windows and Cryogens During Laser Induced Hyperthermia in a Multilayer Vascularized Tissue," Appl. Therm. Eng., **89**(■), pp. 28–35.

[58] Andrieu, C., Doucet, A., Singh, S. S., and Tadic, V. B., 2004, "Particle Methods for Change Detection, System Identification, and Control," Proc. IEEE, **92**(3), pp. 423–438.

[59] Carpenter, J., Clifford, P., and Fearnhead, P., 1999, "An Improved Particle Filter for Non-Linear Problems," IEEE Proc. Radar Sonar Navig., **146**(1), pp. 2–7.

[60] Del Moral, P., and Jasra, A., 2007, "Sequential Monte Carlo for Bayesian Computation," Bayesian Stat., **8**(■), pp. 1–34.

[61] Candy, J. V., 2008, *Bayesian Signal Processing: Classical, Modern, and Particle Filtering Methods*, Wiley, ■.

[62] Kalman, R. E., 1960, "A New Approach to Linear Filtering and Prediction Problems," J. Basic Eng., **82**(1), pp. 35–45.

[63] West, M., 1993, "Approximating Posterior Distributions by Mixture," J. R. Stat. Soc.: Ser. B, **55**(2), pp. 409–422.

[64] Lehikoinen, A., Finsterle, S., Voutilainen, A., Kowalsky, M. B., and Kaipio, J. P., 2009, "Dynamical Inversion of Geophysical ERT Data: State Estimation in the Vadose Zone," Inverse Probl. Sci. Eng., **17**(6), pp. 715–736.

[65] Lipponen, A., Seppänen, A., and Kaipio, J. P., 2011, "Nonstationary Approximation Error Approach to Imaging of Three-Dimensional Pipe Flow: Experimental Evaluation," Meas. Sci. Technol., **22**(10), p. 104013.

[66] Pacheco, C. C., Orlande, H. R. B., Colaço, M. J., and Dulikravich, G. S., 2015, "Estimation of a Location-and-Time Dependent High Magnitude Heat Flux in a Heat Conduction Problem Using the Kalman Filter and the Approximation Error Model," Numer. Heat Transfer, Part A, **68**(11), pp. 1198–1219.

[67] Hasgall, P. A., Di Gennaro, F., Baumgarther, C., Neufeld, E., Gosselin, M. C., Payne, D., Klingenbock, A., and Kuster, N., "IT'IS Database for Thermal and Electromagnetic Parameters of Biological Tissues, Versio 3.0," ■, ■.

[68] Bashkatov, A. N., Genina, E. A., and Tuchin, V. V., 2011, "Optical Properties of Skin, Subcutaneous, and Muscle Tissues: A Review," J. Innovative Opt. Health Sci., **4**(1), pp. 9–38.

[69] Jain, P. K., Lee, K. S., El-Sayed, I. H., and El-Sayed, M. A., 2006, "Calculated Absorption and Scattering Properties of Gold Nanoparticles of Different Size, Shape, and Composition: Applications in Biological Imaging and Biomedicine," J. Phys. Chem. B, **110**(14), pp. 7238–7248.

[70] Prahl, S. A., 1988, "Light Transport in Tissue," Ph.D. thesis, ■, ■. AQ14